Biophysical Journal, Volume *120*

Supplemental information

Integrin-based mechanosensing through conformational deformation

Tristan P. Driscoll, Tamara C. Bidone, Sang Joon Ahn, Alvin Yu, Alexander Groisman, Gregory A. Voth, and Martin A. Schwartz

Supplementary Information

Equilibrium Molecular Dynamics Simulations

We ran 1 μs equilibrium all-atom molecular dynamics (AA MD) simulations on membrane-embedded wild type and mutant $\alpha_V\beta_3$ integrins. The headpiece (from 3IJE.pdb (36)) was connected to its transmembrane helical and cytoplasmic parts (from 2KNC.pdb (37)), resulting in 1780 Cα atoms. Point mutations were selected based on studies that identified mutants with increased affinity for RGD ligands (45): L138I, S243E and K417E. A multicomponent model lipid bilayer with 80% DOPC and 20% DOPS lipids (512 lipids in each leaflet, total 1024 lipids in membrane) was constructed, using CHARMM-GUI membrane builder (33). To hydrate the lipid-membrane/integrin systems, both sides of the lipid bilayer were filled up with TIP3P water molecules and 150 mM NaCl, for a total of about 1.2 million atoms.

Energy minimization was run for 5000 steps of steepest descent algorithm, followed by position restraint in a constant NPT ensemble for 50 ns, using the Berendsen thermostat. Production AA MD simulations were carried out using Gromacs 5.0.4 (42), for 1 μs in the NPT ensemble using Nose-Hoover thermostat and Parrinello-Rahman barostat (43) to keep the temperature at 310 K and pressure at 1 atm with semi-isotropic pressure coupling with a compressibility of $4.5 \times 10^{-5} bar^{-1}$. Long-range electrostatic interactions were incorporated through the Particle Mesh Ewald (PME) method with a cut-off of 1 nm (44). The same cut-off value was used for Lennard-Jones interactions.

Coarse-grained model

Essential Dynamics Coarse-graining (ED-CG) was used to define CG beads for $\alpha_V\beta_3$ integrin. ED-CG is a bottom-up approach which decreases the degrees of freedom of a molecular system by grouping together Cα atoms into CG beads that present correlated displacements during AA MD simulation (32). To evaluate the degree of correlation in Cα atoms motions, a displacement difference was evaluated from the last 400 ns of AA MD. Cα atoms were grouped into CG beads by variationally minimizing the following residual:

$$\chi^2 = \frac{1}{3N}\sum_{I=1}^{N}\frac{1}{N}\sum_{t=1}^{n_t}\left(\left|\Delta r_i^{ED}(t) - \Delta r_j^{ED}(t)\right|^2\right),$$

where *N*=300 is the number of CG beads and $\Delta r_i^{ED}(t)$ is the contribution in the essential subspace from the displacement of residue *i* at time *t*. The more the Cα atoms *i* and *j* moved in a correlated fashion, the more their displacement difference was small, and thus became part of the same CG bead. CG models of WT and mutant $\alpha_V\beta_3$ integrins had average resolution 8 ± 4 Cα atoms (and hence amino acid residues) per CG bead (about 1.2 nm).

Heterogeneous and anharmonic network model

In order to incorporate effective interactions between the CG beads of $\alpha_V\beta_3$ integrin and decrease its bias towards an equilibrium configuration, the modified form of the hENM approach was used (34). First, effective pairwise harmonic interactions between CG-beads below 4 nm cutoff were created as:

$$V(x) = \frac{1}{2}k(x - x_0)^2$$

where k is an effective harmonic spring stiffness, computed based on the average AA fluctuations between pairs of CG beads, and x_0 is equilibrium separation, given by the average AA center of mass distance between all pairs of CG beads. Second, the hENM was used by treating long-range interactions between integrin domains as "softer" dissociable Morse potentials, thus providing flexible and breakable connections between CG beads, such that:

$$V(x) = A_{CG}(1 - e^{(-\alpha(x-x_0))})^2$$

where the dissociation energy, A_{CG}, is the product of a dissociation factor and harmonic spring stiffness resulting from the hENM: $A_{CG} = D \cdot k\,(x_0)$ (58). The dissociation factor, D, was calculated from the exponential of the ratio of averaged distance between non-consecutive, inter-domain distance (approximately 8 nm) to CG resolution (about 1.2 nm): $D = \exp(-< R_{inter} >/< R_{res}^{CG} >) = 0.001.$

Langevin Dynamics of CG systems

To define an open conformation for $\alpha_V\beta_3$ integrins, we used extended $\alpha_{IIB}\beta_3$, mapping the CG representation of bent $\alpha_V\beta_3$ onto open $\alpha_{IIB}\beta_3$, using the center of geometry of corresponding residues. We restrained integrin helices and applied different forces on the ligand binding site, from 1 to 10 pN. All trajectories were obtained using LAMMPS MD software (35) by integrating the Langevin equation of motion with the

temperature set at 310 K, in a constant number of particles, volume, and temperature (NVT) ensemble.

Relation between molecular properties and emergent dynamics of integrin

In our CG models, S243E presented softer effective harmonic potentials (Sup. Fig. 4A-B), and higher equilibrium separations between beads (Sup. Fig. 4C). In order to determine if the reduced spring stiffness' were solely responsible for the observed higher flexibility of S243E at lower forces, we developed models with equilibrium separation between beads from $\alpha_{IIB}\beta_3$ (32). When stretched, these systems extended in proportion to *F*. All mutants extended at least 10% more than WT (Sup. Fig. 4G). At *F* = 1-9 pN, S243E extended more than 15%, while L138I and K417E extended less than 13% (Fig. S2G). S243E was more flexible, more extended and more open than WT and other mutants at low forces. Therefore, the reduced stiffnesses' of the connections between integrin CG beads, regulated by a reduced correlation in residue motions during AA MD simulations, was solely responsible for the increased flexibility of S243E. To summarize, our bottom-up CG model, which was parametrized based on all-atom molecular dynamics simulation data, demonstrated that S243E is uniquely responsive to soft substrates.

Stiffness (Pa)	40% aa (ul)	2% bis-aa (ul)	Water (ul)	APS 10%(ul)	TEMED (ul)
670	75	30	883	10	1.5
4169	125	50	813	10	1.5
11935	187.5	50	751	10	1.5
25176	187.5	150	651	10	1.5
47626	300	75	613.5	10	1.5

Supplemental Table 1: PA gel composition for imaging

Stiffness (Pa)	40% aa (ul)	2% bis-aa (ul)	60% NHS acrylate (ul)	Citric buffer (pH 4) (ul)	APS (ul)	TEMED (ul)
490	45	7.5	33	394	20	1
5083	84	11	62	323	20	1
30027	135	37.5	100	208	20	1

Supplemental Table 2: PA gel composition for western blots

Supplementary Figures

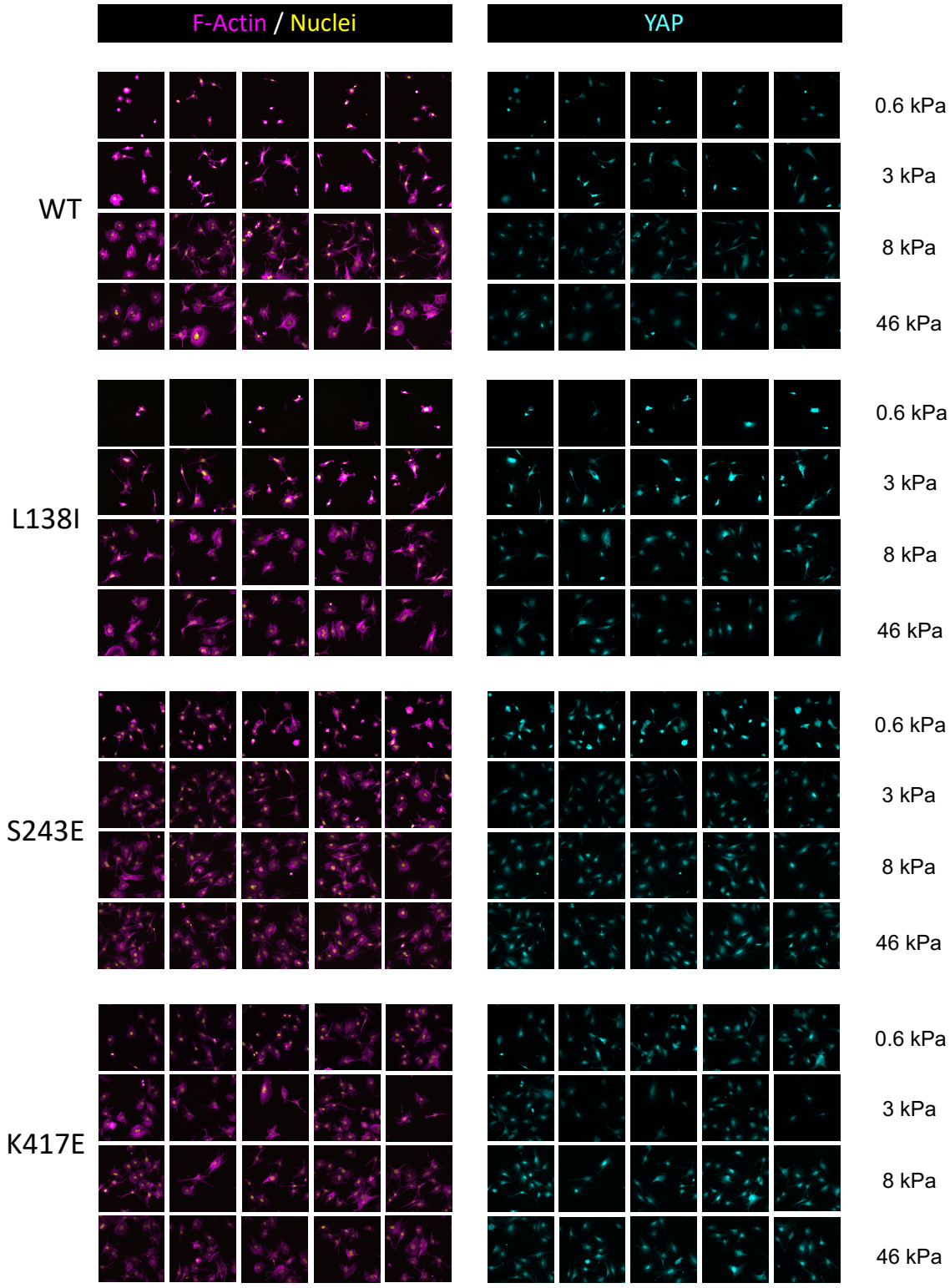

Supplemental Figure 1. MLEC Spread Area and YAP

Example images for WT and mutant integrin (L138I, S243E, K417E) cells seeded on fibrinogen coated PA gels of varying stiffness (0.6, 3, 8, 46, kPa). Images on the left show F-actin (phalloidin) in magenta and nuclei (DAPI) in yellow. Images on the right show YAP in cyan.

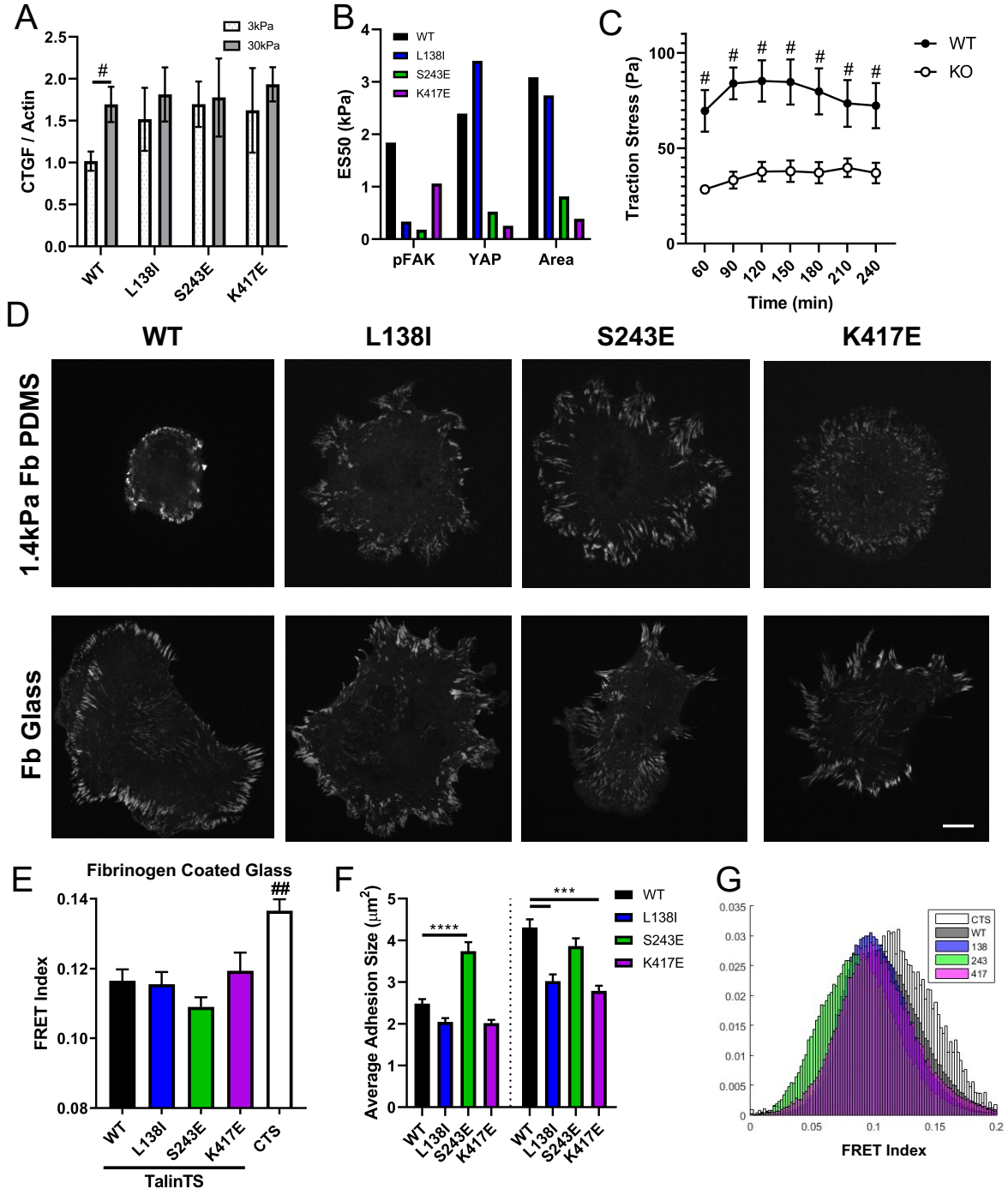

Supplemental Figure 2. MLEC control data

(A) qPCR of the YAP target gene CTGF normalized to β-Actin for WT or mutant cells seeded on fibrinogen coated 3 or 30kPa silicone gels for 24 hours (mean +/- SEM, n=4 independent samples per group from 2 experiments, # $p<0.05$ two-way ANOVA with Tukey's post hoc). (B) Calculation of the effective stiffness required for 50% activation of pFAK, YAP, and spread area based on fitting of normalized response data at each stiffness for WT and mutant cells using the Hill equation. (C) Average traction stress from traction force microscopy on 11kPa fibrinogen coated pluronic blocked silicone gels seeded for 75-240 minutes. (# $p<0.01$, unpaired t-test's, mean ± SEM, n=17-24 cells per group from 2 independent experiments). (D) Representative images of GFP Talin tension sensor with quantification (F) of talin adhesion size on fibrinogen coated 1.4kPa silicone and glass with (mean +/- SEM, n=349-961 adhesions per group, scale bar = 10μm, * $p<0.05$, *** $p<0.01$, **** $p<0.0001$, Kruskal-Wallis test with Dunn's post hoc). (E) Quantified FRET index for talinTS or CTS in WT or mutant cells on Fibrinogen coated glass (mean+/- SEM, n=12-20 cells per group from two independent experiments, ## $p<0.01$ for control sensor vs. all groups, one-way ANOVA with Tukey's post hoc). Differences in FRET index between WT and mutants not significant. (G) Pixel histograms for FRET index data shown in Fig. 3C (n=7-10 cells per group).

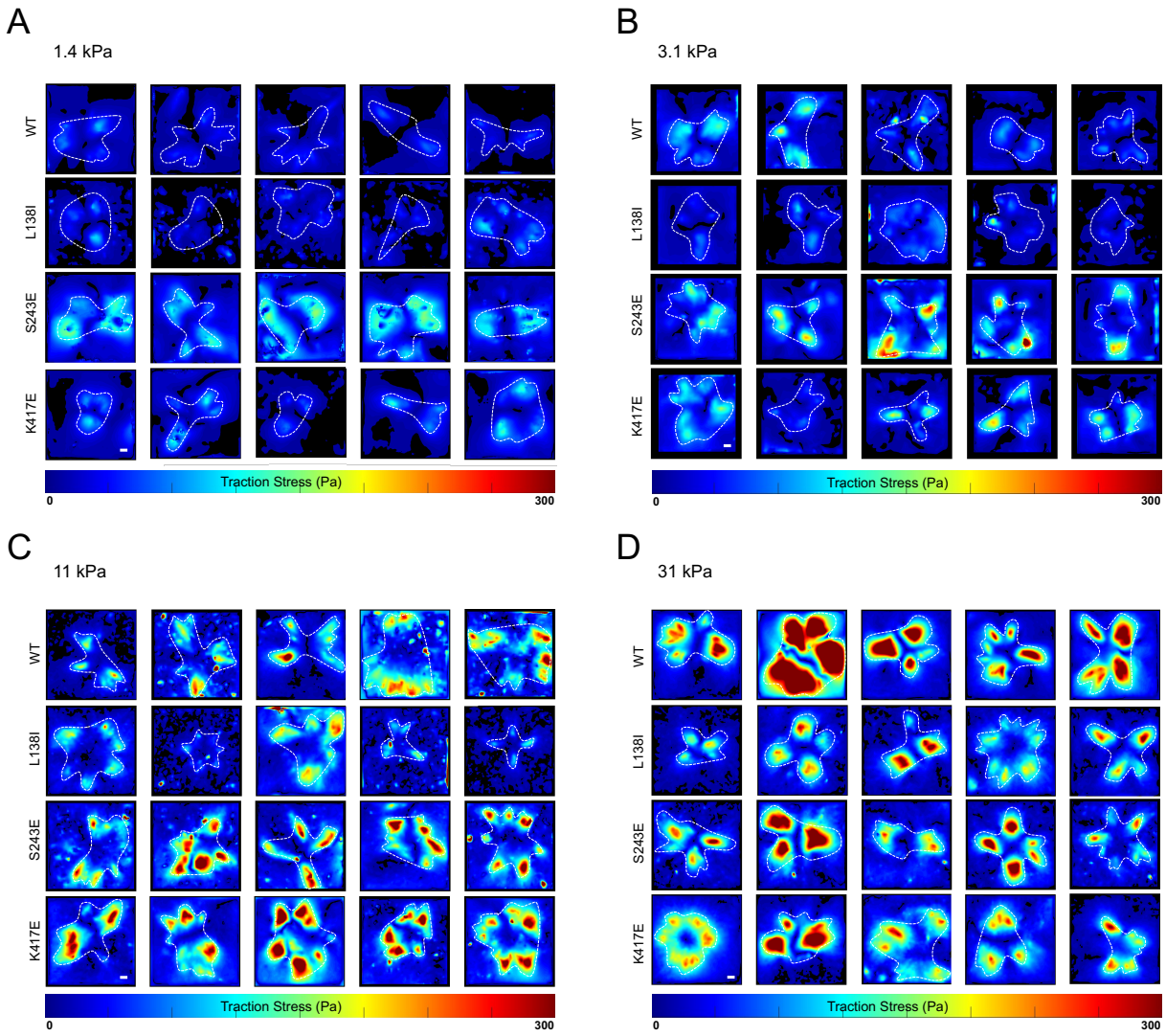

Supplemental Figure 3. Traction force microscopy heatmaps

Stress heatmaps for 5 representative cells for each group, WT or mutant cells on 1.4kPa (A), 3.1kPa (B), 11kPa (C), 31kPa (D) (scale bar = 10μm).

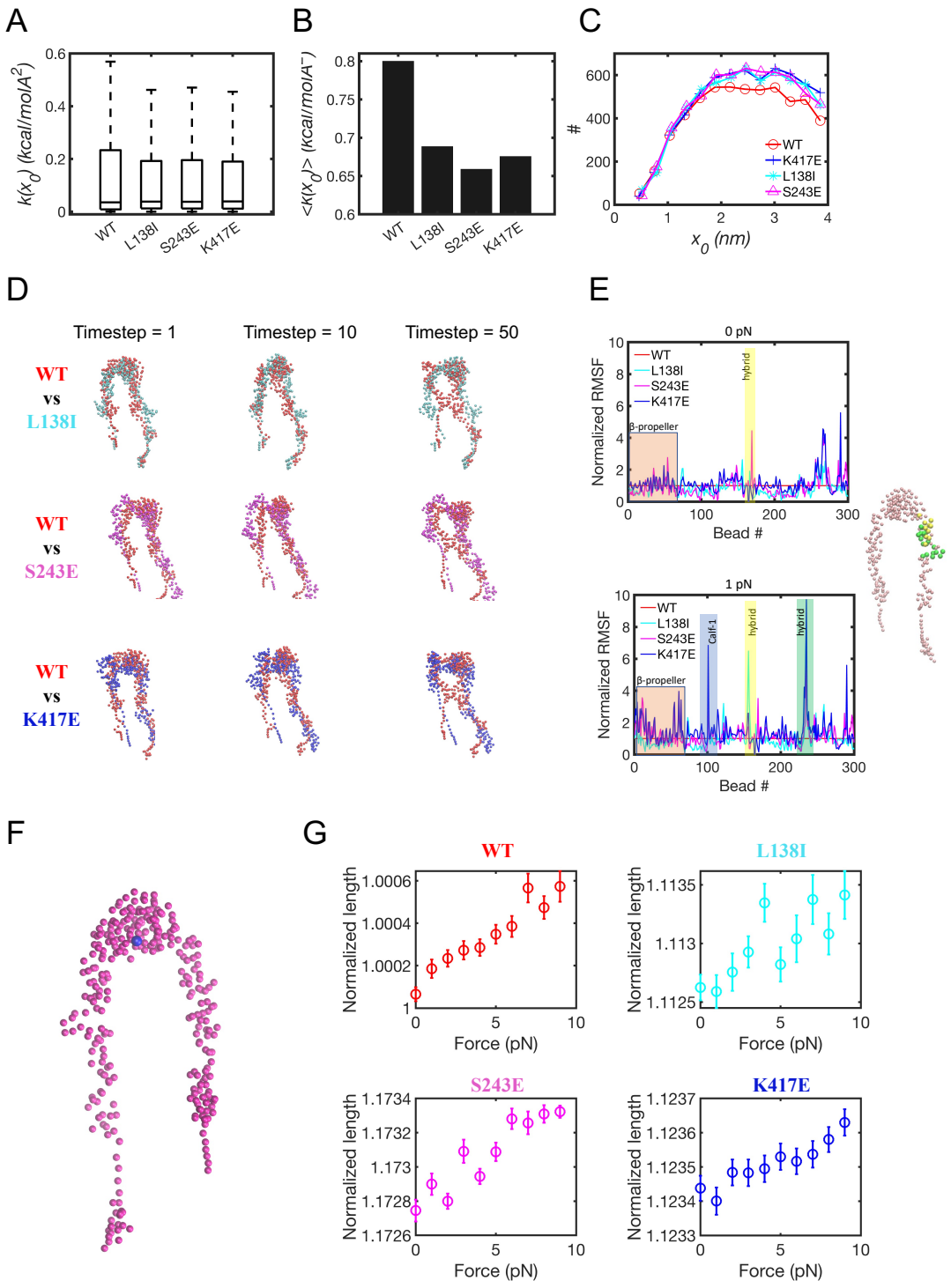

Supplemental Figure 4. Calculated flexibility for integrin mutants.

(A) Distributions of spring constants for the CG models of WT and mutant integrins. **(B)** Average spring constants, *k*, for CG models of WT and mutant integrins. **(C)** Distribution

of equilibrium separations between beads, x_0, for CG models of WT and mutant integrins. **(D)** Snapshots of the simulations at different timesteps, where the mutants (cyan, magenta and blue) are overlaid to WT (in red). **(E)** Root mean square fluctuations (RMSF) of CG models of WT and mutant integrins at F = 0 pN and F = 1 pN. All values are normalized by RMSF of WT integrin. At F = 0 pN, $p<0.05$ between mutants; at F = 1 pN, $p<0.001$ between mutants. CG model of wild type extended integrin is reported on the right, with the two groups of beads corresponding to the two groups of residues of the hybrid domain highlighted in yellow and green**. (F)** CG model of extended integrin with equilibrium separation between beads from $\alpha_{IIB}\beta_3$. **(G)** Normalized force-extension relations for CG models of WT and mutant integrins.